# Protecting Hilbert space fragmentation through quantum Zeno dynamics

Pranay Patil [1,*] Ayushi Singhania [2,†] and Jad C. Halimeh[3,4,‡]

[1]*Max Planck Institute for the Physics of Complex Systems, 01187 Dresden, Germany*
[2]*Institute for Theoretical Solid State Physics, IFW Dresden, 01069 Dresden, Germany*
[3]*Department of Physics and Arnold Sommerfeld Center for Theoretical Physics (ASC), Ludwig-Maximilians-Universität München,*
*D-80333 München, Germany*
[4]*Munich Center for Quantum Science and Technology (MCQST), D-80799 München, Germany*

Hilbert space fragmentation is an intriguing paradigm of ergodicity breaking in interacting quantum many-body systems with applications to quantum information technology, but it is usually adversely compromised in the presence of perturbations. In this work, we demonstrate the protection of constrained dynamics arising due to a combination of mirror symmetry and Hilbert space fragmentation by employing the concept of quantum Zeno dynamics. We focus on an Ising spin ladder with carefully chosen quantum fluctuations, which in the ideal case guarantee a perfect disentanglement under Hamiltonian dynamics for a large class of initial conditions. This is known to be a consequence of the interplay of Hilbert space fragmentation with a mirror symmetry, and we show numerically the effect of breaking the latter. To evince the power of this perfect disentanglement, we study the effect of generic perturbations around the fine-tuned model and show that we can protect against the undesirable growth of entanglement entropy by using a local Ising interaction on the rungs of the ladder. This allows us to suppress the entanglement entropy to an *arbitrarily* small value for an *arbitrarily* long time by controlling the strength of the rung interaction. Our work demonstrates the experimentally feasible viability of quantum Zeno dynamics in the protection of quantum information against thermalization.

## I. INTRODUCTION

One of the most intriguing questions in quantum many-body physics is the nature of thermalization, or its absence, in an isolated quantum system [1,2]. Although generic quantum many-body models satisfying the eigenstate thermalization hypothesis are expected to thermalize at sufficiently long times [3–5], examples abound where interacting systems do not seem to thermalize for all accessible evolution times. For instance, many-body localization (MBL) has been argued to exist in the presence of a disorder potential [6–10] or a sufficiently strong Stark potential in an otherwise translation-invariant system [11,12]. In the context of gauge theories, disorder-free localization can arise due to the plethora of conserved local constraints when the initial state spans an extensive number of gauge superselection sectors [13–15], and the presence of such a substructure can be diagnosed using spectral signatures [16,17]. In certain nonintegrable

models, initial states prepared in a cold subspace of quantum many-body scars—nonthermal eigenstates with anomalously low bipartite entanglement entropy and roughly equal energy spacing—lead to long-lived oscillations in the dynamics of local observables persisting beyond all relevant timescales and avoiding thermalization [18–21].

Recently, an exciting paradigm of ergodicity breaking known as Hilbert space fragmentation (HSF) has emerged, first reported for systems with dipole conservation [22,23] where HSF can be fully characterized by nonlocal integrals of motion [24]. More generally, it was found that this phenomenon consists of the Hilbert space fragmenting into an exponentially large number of invariant subspaces resulting from an exponentially large number of commutant algebras [25]. HSF has received significant recent attention, with theoretical works demonstrating its presence in models with strict confinement [26,27], including gauge theories with a topological $\theta$ term [27,28], and it has been the focus of several recent ultracold-atom experiments [29,30]. A coupling between HSF and spatial fragmentation [31] can allow for real space fragmentation and this can be exploited to control the spread of entanglement.

The sensitivity of HSF to perturbations has been highlighted since its introduction, where terms that violate local constraints have been shown to lead to eventual thermalization at sufficiently long times [22,32]. This sensitivity of HSF is disadvantageous from a fundamental point of view and for possible applications in quantum technology, and therefore it is important to investigate means of protecting dynamical

---

*patil@pks.mpg.de
†singhania@ifw-dresden.de
‡jad.halimeh@physik.lmu.de

features of HSF. In this paper, we explore the concept of quantum Zeno dynamics (QZD) [33–36] in extending the lifetime of HSF-induced phenomena. In particular, we expand on a recently proposed model [31] which exploits HSF and spatial symmetry to engineer preservation of a perfectly disentangled structure for a large class of initial product conditions. This model is a special case of a quantum compass model [37,38], and it has been investigated in the one-dimensional (1D) case using an exact Jordan-Wigner transformation to free fermions [39], as a realization of MBL physics in a system free of disorder. This leads to no entanglement developing under Hamiltonian dynamics for particular spatial regions, which is a unique aspect of this model not found in general models exhibiting HSF.

Although the model is fine-tuned, we show here that engineering large energy-scale separations by adding simple local interaction terms is able to thwart the growth of entanglement entropy (EE) due to perturbations that would otherwise render the model generically chaotic. This treatment goes beyond the particular 1D case studied using a mapping to free fermions in Ref. [39], as it tackles generic perturbations which break integrability and is applicable for bilayer lattices in general dimension with arbitrary connectivity. Our results have implications in two important ways. First, it illuminates the effect of a simple symmetry on the avoidance of thermalization. Second, from a quantum-information perspective, it outlines a method of protecting against unwanted entanglement buildup between different spatially separated parts of a quantum circuit, which can be useful in error mitigation. The crucial difference with previous attempts [40] to engineer prethermal behavior using Zeno dynamics is that here we are able to stabilize a "useful" state, i.e., one which has entanglement structure similar to a product state. This is qualitatively different from a generic prethermal state which lacks spatial fragmentation.

The rest of the paper is organized as follows: We begin in Sec. II by describing the model and the mechanism by which it prevents spread of entanglement entropy. This is followed by a discussion of the importance of local conserved quantities and a spatial mirror symmetry, and we show numerically the effect of breaking the latter. In Sec. III we discuss simple perturbations which break the local conservation and introduce a growth of EE, and propose a simple protection scheme based on QZD to suppress this growth. We justify our choice by studying the structure of the energy spectrum and show numerically that its strength controls parametrically the value and lifetime of a stable and suppressed EE plateau. This leads to scaling relations between the value of EE, the perturbation strength, and the coefficient of the protection term, and we present analytic arguments from perturbation theory to justify them in Sec. IV. We conclude and discuss future directions in which our results can be extended in Sec. V.

## II. UNPERTURBED MODEL $\hat{H}_0$

We shall now discuss one of the simplest manifestations of the properties we require to prevent the spread of entanglement in a quantum many-body system, which is through a model of coupled Ising spins with Hamiltonian

$$\hat{H}_0 = -J \sum_i \left( \hat{\sigma}_i^z \hat{\sigma}_{i+1}^z + \hat{\tau}_i^z \hat{\tau}_{i+1}^z + \hat{\sigma}_i^x \hat{\tau}_i^x \right), \quad (1)$$
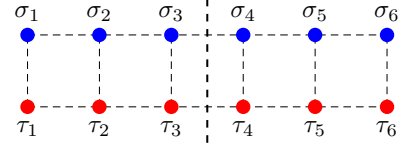


FIG. 1. Schematic picture of a spin system hosting two sets of identical spins ($\sigma$ and $\tau$) in a ladder geometry with a Hamiltonian given by Eq. (1). Vertical dashed line across the center represents the partition across which entanglement entropy is calculated.

where the spin species are labeled by operators $\hat{\sigma}_i^a$ and $\hat{\tau}_i^a$ on site $i$ with $a = x, y, z$, and with eigenvalues $\sigma_i^a$ and $\tau_i^a$, respectively. The energy scale is set by $J = 1$. This model was first discussed in Ref. [31] for general lattices. For ease of numerical investigation, we shall here restrict our system to be a ladder with open boundary conditions, see Fig. 1. Hamiltonian (1) conserves $\hat{\sigma}_i^z \hat{\tau}_i^z$ on each rung—$[\hat{H}_0, \hat{\sigma}_i^z \hat{\tau}_i^z]=0$, $\forall i$—leading to a fragmentation of the Hilbert space into $2^N$ fragments, where $N$ is the system size. Let us now restrict ourselves to one such sector, which can be represented as a particular assignment for $\sigma_i^z \tau_i^z$ such as $\dots + + + - - + + + + + -$ $- + - - - - - \dots$, where $+(-)$ corresponds to $\sigma_i^z \tau_i^z = \pm 1$, and we shall denote an eigenvalue $\sigma_i^z$ or $\tau_i^z$ with a value $+(-)$ by 1(0) for ease of notation. For a rung, which hosts $+(-)$, $(\sigma_i^z, \tau_i^z)$ can thus be 00(01) or 11(10).

Note that under an exchange of $\hat{\sigma}_i^a \leftrightarrow \hat{\tau}_i^a$, the states in the $(\hat{\sigma}_i^z, \hat{\tau}_i^z)$ basis corresponding to $\sigma_i^z \tau_i^z = +1$ are invariant, i.e., $00(11) \to 00(11)$, whereas those for $\sigma_i^z \tau_i^z = -1$ are interchanged, i.e., $01(10) \to 10(01)$. Now note that the term $\hat{H}_d = -J \sum_j (\hat{\sigma}_j^z \hat{\sigma}_{j+1}^z + \hat{\tau}_j^z \hat{\tau}_{j+1}^z)$ of Hamiltonian (1) is diagonal in the $(\hat{\sigma}_i^z, \hat{\tau}_i^z)$ basis and is symmetric under $\hat{\sigma}_i^a \leftrightarrow \hat{\tau}_i^a$. This is the crucial property that we will exploit, which implies that our argument should hold for any diagonal operator with this property. Consider now neighboring rungs $i$ and $i + 1$ that host $+-$ as their respective assignment of the conserved quantity. This would imply that the matrix elements of the inter-rung diagonal interaction, $\langle (00)_i (01)_{i+1} | \hat{H}_d | (00)_i (01)_{i+1} \rangle$ and $\langle (00)_i (10)_{i+1} | \hat{H}_d | (00)_i (10)_{i+1} \rangle$, are equivalent under $\hat{\sigma}_i^a \leftrightarrow \hat{\tau}_i^a$, which is a symmetry of the full Hamiltonian. This means that there is effectively no interaction between neighboring rungs that host different values for $\sigma^z \tau^z$. As such, the effective system within this sector breaks up into smaller spatial segments given by the corresponding arrangement of $\sigma_i^z \tau_i^z$. The Hamiltonian in this sector can now be written as

$$\hat{H}_{\text{sector}} = -J \sum_s \left[ \sum_{\langle i,j \rangle \in s} \left( \hat{\sigma}_i^z \hat{\sigma}_j^z + \hat{\tau}_i^z \hat{\tau}_j^z \right) + \sum_{i \in s} \hat{\sigma}_i^x \hat{\tau}_i^x \right], \quad (2)$$

where $s$ labels the different strings into which the sector is broken. For example, a sector labeled by $+ - - - + + - -$ would be made up of four noninteracting strings with one site, three sites, two sites, and two sites, respectively. This feature has already been understood in Ref. [31] and explored as a special limit of the more general model in Ref. [39].

Furthermore, the spatial decoupling discussed above leads to a $\mathbb{Z}_2$ Ising symmetry associated with each string. This implies that the sector breaks up further into $2^{N_s}$ subsectors, where $N_s$ is the number of strings. One can construct the conserved quantities associated with these subsectors using
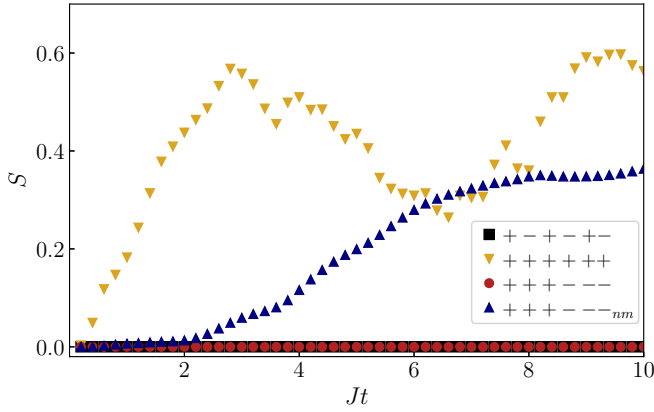
FIG. 2. Growth of the midchain EE for $\hat{H}_0$ for various sectors labeled by the set of eigenvalues ($\pm 1$) of $\hat{\sigma}_i^z \hat{\tau}_i^z$. Sectors with differing values across the middle develop no entanglement under Hamiltonian time evolution (see text). The subscript *nm* signifies "no mirror," i.e., the system without a mirror symmetry, which does not allow for a protection of information (see text).

the methodology developed in Ref. [25], and these correspond to products of $\hat{\sigma}_i^x \hat{\tau}_i^x$ on a string and projectors to the domain wall which forces the $+-$ pattern at the ends of the string of rungs.

We can now consider a product initial state restricted to such a sector. On undergoing Hamiltonian dynamics, the corresponding growth of EE is now going to be limited to small spatial segments, and genuine volume-law EE can never develop. We verify this numerically for a six-rung ladder corresponding to 12 spins, see Fig. 1, by considering random product states in sectors such as $+-+-+-$ and $+++-$ $--$, and find that the half-chain (corresponding to a $+-$ wall) EE to be exactly zero for all times, as shown in Fig. 2. We generate our random product states, as done in Ref. [41] by choosing a random $(\theta_i, \phi_i)$ for rung number $i$, and initializing the $(\sigma, \tau)$ pair on that rung as $\cos\theta_i|00\rangle + \sin\theta_i e^{i\phi_i}|11\rangle$ if the sector constraint is $\sigma_i^z \tau_i^z = +1$ on that rung or as $\cos\theta_i|01\rangle + \sin\theta_i e^{i\phi_i}|10\rangle$ if $\sigma_i^z \tau_i^z = -1$.

In contrast, a sector such as $+++++$ or $++++--$ develops partial half-chain EE in the long-time limit. For the rest of this paper, we shall study only the half-chain EE. To emphasize the importance of the $\hat{\sigma}_i^a \leftrightarrow \hat{\tau}_i^a$ (mirror across rungs) symmetry, we show the dynamics of the EE under Hamiltonian (1) with the additional $-0.1 \sum_{\langle i \rangle} \hat{\tau}_i^z \hat{\tau}_{i+1}^z$, which breaks this mirror symmetry. Using the sector $+++---$ for our simulation, we find, as shown in Fig. 2, that there is a growth of EE that was not present for the symmetric Hamiltonian. As such, the requirement for the $\hat{\sigma}_i^a \rightarrow \hat{\tau}_i^a$ mirror symmetry is absolute, i.e., if we lose this property, every sector behaves as a generic many-body system, which builds volume-law EE in the long-time limit. However, this simply implies the requirement of a spatial symmetry, which is generally expected for periodic crystals. Although the results for the 1D case we have presented above can be understood as a special case of the spin ladder discussed in Ref. [39], we emphasize here that the spatial fragmentation holds for general dimension, and our numerical studies are restricted to the 1D case purely due to inability of an efficient algorithm

to simulate exact quantum dynamics of a large number of interacting spins. The results of the current and the following sections are applicable to higher dimensional lattices and should not be considered to be specific to the 1D case, as is often the case in quantum dynamics.

## III. PROTECTION WITH QUANTUM ZENO DYNAMICS

Let us now consider perturbations $\hat{H}_1$ that are off-diagonal in the $(\hat{\sigma}^z, \hat{\tau}^z)$ basis. These terms do not affect the perfect mirror symmetry of $\hat{\sigma}_i^z \leftrightarrow \hat{\tau}_i^z$, but destroy the conservation of $\hat{\sigma}_i^z \hat{\tau}_i^z$ on each rung and thereby enhance the quantum dynamics and destroy HSF. This occurs due to a loss of sector structure, and thus a leakage of EE due to a sector with the $\sigma_i^z \tau_i^z$ assignment of the form $\ldots + - \ldots$ is able to transition to one with an assignment of $\ldots + + \ldots$, where entanglement can build up between the two relevant sites. In the following, we will consider two such perturbations, both of which mix all sectors in such a way, leading to the EE of a random state [42] in the Hilbert space in the long-time limit.

We can now employ the concept of QZD [33–36] in order to protect the constrained dynamics arising originally due to HSF and mirror symmetry in $\hat{H}_0$. Although Zeno dynamics is usually understood in the context of rapid measurement of the system leading to restricted dynamics due to effective projection, it can also be understood using a rotating reference frame, which protects against the effect of perturbations which are off-resonance [40]. In this case, the high-frequency rotation acts as a projection into the rotating frame, thus functionally behaving as a series of rapid measurements. QZD allows us to project the Hamiltonian dynamics into the sector of choice, thus negating the effect of the perturbation $\hat{H}_1$. This can be achieved by adding a *protection* term $\hat{H}_V$ diagonal in the $(\sigma^z, \tau^z)$ basis with strength $V$, which is the largest energy scale in our Hamiltonian. This term is chosen to have a spectrum that forms plateaus, such that all the $(\sigma^z, \tau^z)$ basis vectors in a sector generate the same expectation value for $\hat{H}_V$ (spectrum shown in Fig. 3). Note that this implies that each sector corresponds to only one plateau, but each plateau can contain many sectors. Now the energy separation between different plateaus leads to a suppression of inter plateau dynamics [35], and thus a suppression of intersector dynamics, provided the sectors are in different energy plateaus. Note that the suppression of intersector dynamics is perfect only for $V \rightarrow \infty$, that for any finite value of $V$ we should expect some small renormalized value for the EE, and that it would last only up to a finite time, until which point the dynamics accumulates enough leakage out of the sector and leads to thermalization. Indeed, from QZD one obtains an effective Zeno Hamiltonian $\hat{H}_Z = \hat{H}_0 + \sum_S \hat{\mathcal{P}}_S \hat{H}_1 \hat{\mathcal{P}}_S$ that faithfully reproduces the HSF dynamics up to timescales at the earliest linear in $V$, where $\hat{\mathcal{P}}_S$ is the projector onto the quantum Zeno subspace **S** [33]. The Zeno Hamiltonian further reduces to $\hat{H}_Z = \hat{H}_0 + \hat{\mathcal{P}}_{S_0} \hat{H}_1 \hat{\mathcal{P}}_{S_0}$, when the initial state is prepared in a given Zeno subspace $S_0$.

To design a protection term particularly well suited to prevent the growth of entanglement starting from a specific sector, we must bias it towards the configuration of $\sigma_i^z \tau_i^z$ corresponding to this sector. This can be done by choosing $\hat{H}_V = V \sum_i c_i \hat{\sigma}_i^z \hat{\tau}_i^z$, where $c_i = \pm 1$, depending on the sector
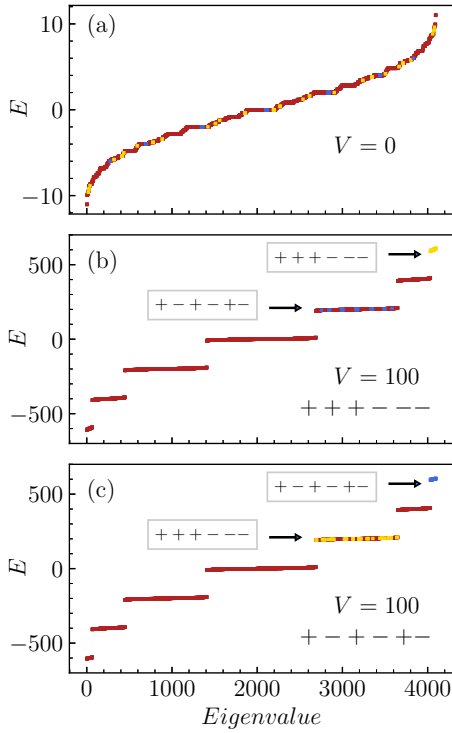
FIG. 3. Energy spectrum of 12-site system ($L = 6$ rungs) with $\lambda = 0$, (a) $V = 0$, (b) $V = 100$ with $c_i \in \{+1, +1, +1, -1, -1, -1\}$, and (c) $V = 100$ with $c_i \in \{+1, -1, +1, -1, +1, -1\}$. The yellow and blue colors correspond to states in the sectors $+ + + - - -$ and $+ - + - + -$, respectively. For $V = 0$, it can be clearly seen that there is no energetic separation between various sectors, and the dynamics is restricted only by the conserved quantities, whereas for $V \gg J = 1$, the large energy separation ensures protection against perturbations with the correct sequence $c_i$. Note that the spectra shown in panels (b) and (c) show little difference to the case with a finite nonzero $\lambda \ll V$.

assignment. For example, for an assignment of $+ + + - - -$, we would have $c_i \in \{+1, +1, +1, -1, -1, -1\}$. This choice of $c_i$ completely energetically isolates the sector—rendering it a unique Zeno subspace $\mathbf{S}_0$—as all other assignments must necessarily frustrate one of the $c_i$, leading to a shift to a different plateau. The next closest sector, created by toggling a single $+ \leftrightarrow -$, is thus separated in the spectrum by an energy gap of $2V$. Figure 3 shows the energy spectrum for $\hat{H}_0$ and $\hat{H}_V$, with two different target sectors highlighted. First consider Fig. 3(a), where the spectrum of $\hat{H}_0$ is shown. Here we see that there is no energy separation between different sectors and thus sectors are protected against mixing only by the local conservation of $\sigma_i^z \tau_i^z$. The introduction of a large $V$ leads to a clear separation of the spectrum into plateaus, with the targeted sector floating to the top of spectrum and being well separated from all other sectors. However, nontargeted sectors remain in the middle of the spectrum, sharing energy levels with other sectors. These features can be seen in Figs. 3(b) and 3(c). In this section, we find that such an energy separation translates dynamically into a prethermal regime due to projective quantum Zeno dynamics, which can be seen as a plateau in EE with a tunable value and lifetime. The prethermal plateau is expected to exist for systems on

general lattices, described by the Hamiltonian discussed above, as the protection term and the perturbations are both local and a pattern for conserved charge can be defined thus in a straightforward manner [31].

In Secs. III A and III B, we consider two different forms for the perturbation $\hat{H}_1$, and numerically investigate their effect on EE growth in different sectors under specific protection for these sectors. The numerical results in these subsections show the occurrence of the EE plateau discussed above. In Sec. III C, we examine the lifetime of this prethermal plateau and show that its qualitative dependence on $V$ depends on the structure of the given sector that we choose to protect. In Sec. III D, we investigate the degree of protection that a particular choice of terms can offer to sectors it is not explicitly designed to protect, and its dependence on the type of perturbation used. We close this section by discussing our results in the thermodynamic limit in Sec. III E, where we use the time-dependent variational principle (TDVP) algorithm [43–46] to simulate larger system sizes.

### A. Transverse-field perturbation

Let us examine the quench dynamics under $\hat{H} = \hat{H}_0 + \hat{H}_1 + \hat{H}_V$ with a simple global transverse-field perturbation $\hat{H}_1 = \lambda \sum_i (\hat{\sigma}_i^x + \hat{\tau}_i^x)$, which violates the local conservation of $\sigma_i^z \tau_i^z$ by toggling its value on a single rung from $+ \leftrightarrow -$. This allows transitions, e.g., from "insulating" sectors of the type $+ + + - - -$ to "conducting" ones of type $+ + + + - -$. We study the suppression of EE for initial product states belonging to the sectors $+ + + - - -$ and $+ - + - + -$, both of which prevent entanglement buildup across the center of the chain in the ideal case of $\lambda = 0$, by implementing protection terms specific to these sectors as discussed above. The results for the half-chain EE from exact diagonalization of a 12-spin (6-rung) system are shown in Figs. 4 and 5 for a range of $\lambda$ and $V$ values. Note that we see a plateau with a small value of EE from intermediate to large values of $Jt$ that scales $\propto \lambda^2 / V^2$. This plateau eventually leads to a slow growth of the EE to the saturation value, which is expected to be proportional to the system volume [42]. The value of the EE at the plateau can be clearly seen to decrease quadratically with increasing values of $V/\lambda$. This behavior can be intuitively understood by considering the $V$ and $\lambda$ terms to have opposing effects, i.e., the perturbation promotes a spread of the wave function into other sectors, in which entanglement can be built up, whereas the protection term projects it back into the sector of interest according to QZD. The insets in Figs. 4 and 5 show a data collapse by rescaling the EE by $(V/\lambda)^2$. An analytic understanding of this scale is provided by a perturbation theory analysis in Sec. IV. Note that there is no significant difference between the behavior of the EE for the sectors $+ + + - - -$ (Fig. 4) and the sector $+ - + - + -$ (Fig. 5), as in each case the protection term is appropriately chosen.

### B. Heisenberg perturbation

For a perturbation of the form $\hat{H}_1 = \lambda \sum_i (\hat{\sigma}_i^x \hat{\sigma}_{i+1}^x + \hat{\sigma}_i^y \hat{\sigma}_{i+1}^y + \hat{\tau}_i^x \hat{\tau}_{i+1}^x + \hat{\tau}_i^y \hat{\tau}_{i+1}^y)$, we find that the EE behaves in a manner similar to the case of the transverse-field perturbation, as demonstrated in Figs. 6 and 7 for initial product states in
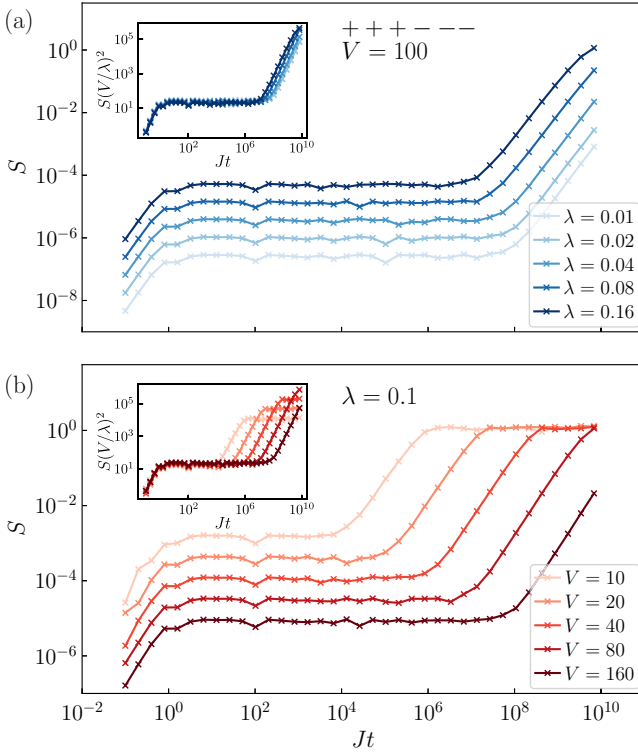
FIG. 4. Entanglement entropy growth for a product initial state in the $+++---$ sector with $c_i \in \{+1, +1, +1, -1, -1, -1\}$ in the presence of the transverse-field perturbation. (a) Varying $\lambda$ for $V = 100$ or (b) varying $V$ for $\lambda = 0.1$ shows a prethermal plateau in the EE whose value and duration is controlled by $(V, \lambda)$ leading to a controllable suppression of the EE. The insets show the EE rescaled by $(V/\lambda)^2$, signifying the value of the EE prethermal plateau $\propto \lambda^2/V^2$.

the sectors $+++---$ and $+-+-+-$. This Heisenberg perturbation term acts by toggling the value of $\sigma_i^z \tau_i^z$ on neighboring rungs. We show in Figs. 6 and 7 the growth of the EE for various values of $V$ and $\lambda$, where once again we find a convincing data collapse by rescaling the EE by $(V/\lambda)^2$. We therefore see that the protection term $\hat{H}_V$, for an appropriate sequence $c_i$, will stabilize HSF-induced constrained dynamics with the EE exhibiting a plateau $\propto \lambda^2/V^2$ up to times linear in $V$ in a worst-case scenario. This shows that the protection term is able to reliably stabilize the system against different types of perturbations.

### C. Lifetime of prethermal plateau

Let us now take a closer look at the timescales of the EE plateaus shown in Figs. 4–7. As we have previously mentioned, a properly chosen sequence $c_i$ allows the protection term $\hat{H}_V$ to induce QZD dynamics that reliably and controllably stabilizes the EE into a plateau of value $\propto \lambda^2/V^2$ up to a timescale that is, in the worst-case scenario, linear in $V$ [33]. By properly rescaling the time axes, Fig. 8 illustrates the timescales of the EE plateaus resulting from the dynamics shown in Figs. 4–7. In the case of the transverse-field perturbation, we observe that when we target the sector $+++---$, a rescaling of the time axis to $\lambda(J/V)^3 t$,
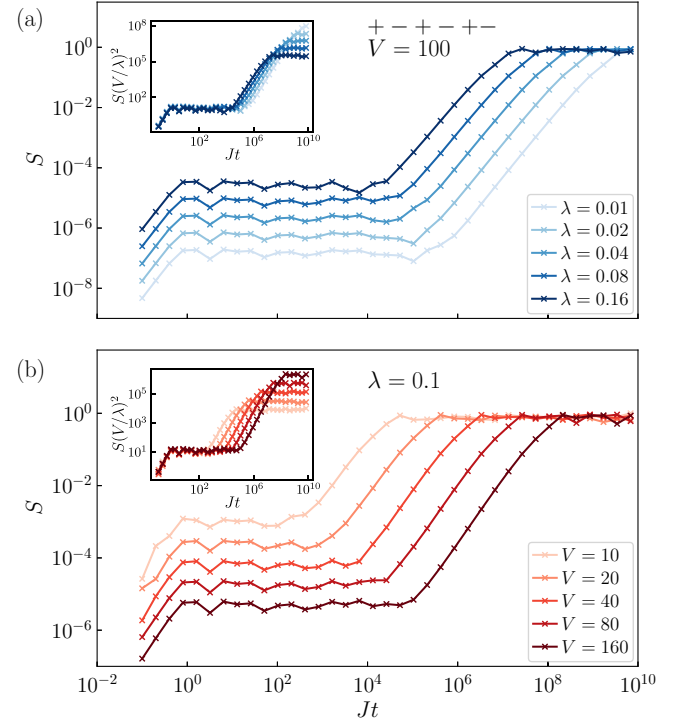


FIG. 5. Entanglement entropy growth for a product initial state in the sector $+-+-+-$ with $c_i \in \{+1, -1, +1, -1, +1, -1\}$ in the presence of the transverse-field perturbation. (a) Varying $\lambda$ for $V = 100$ or (b) varying $V$ for $\lambda = 0.1$ show similar features as Fig. 4. The insets show the rescaled EE, indicating that the EE settles into a prethermal plateau $\propto \lambda^2/V^2$.

results in a convincing data collapse for the complete range of $(\lambda, V)$ which we have studied, indicating a timescale of the EE plateau $\propto V^3/(J^3\lambda)$, which is significantly better than the linear-in-$V$ worst-case prediction from QZD. For the sector $+-+-+-$, we find that we must modify our scaling to $\lambda(J/V)^2 t$, leading to a plateau timescale $\propto V^2/(J^2\lambda)$, also exceeding the QZD prediction. For the Heisenberg perturbation, the plateau timescale for the initial state in the sector $+++---$ is $\propto V^2/(J^2\lambda)$ and for the initial state in the sector $+-+-+-$ is $V/(J\lambda)$, implying a more adverse effect of this perturbation than its transverse-field counterpart. We note that such a difference in the Zeno timescales based on the type of error has also been reported in the context of lattice gauge theories [40].

### D. Protection of nontargeted sectors

Here we examine the extent to which our protection term can protect sectors for which it is not specifically designed to protect. As seen in the spectrum shown in Fig. 3(c), an example of such a sector would be $+-+-+-$. We reiterate that the protection term corresponding to the spectrum here contains the sequence $c_i \in \{+1, +1, +1, -1, -1, -1\}$, and thus does not follow the configuration of the sector we wish to protect. However, it is still possible to prevent a growth of EE for perturbations that are unable to connect sectors lying in the same energy plateau. An example of such a perturbation is the transverse-field term $\hat{H}_1 = \lambda \sum_i (\hat{\sigma}_i^x + \hat{\tau}_i^x)$ discussed in
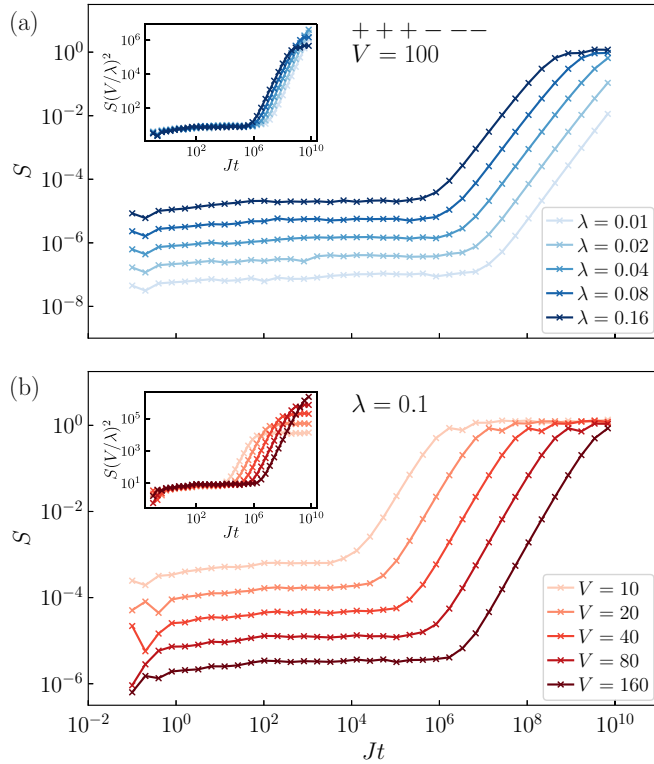
FIG. 6. Entanglement entropy growth for a product initial state in the sector $+++---$ with the Heisenberg perturbation and with $c_i \in \{+1, +1, +1, -1, -1, -1\}$. (a) Varying $\lambda$ for $V = 100$ or (b) varying $V$ for $\lambda = 0.1$, shows a controlled prethermal EE plateau $\propto \lambda^2/V^2$. The insets show the rescaled EE.
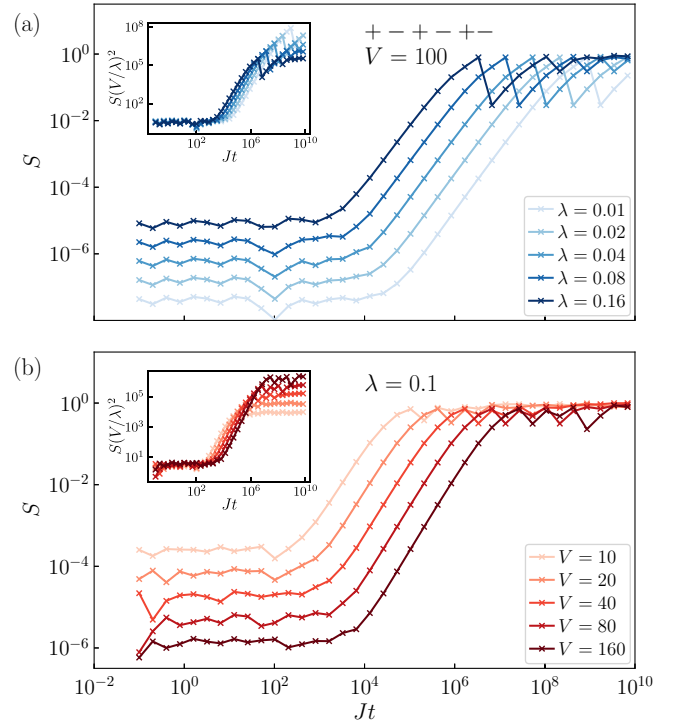


FIG. 7. Entanglement entropy growth for a product initial state in the sector $+-+-+-$ and $c_i \in \{+1, -1, +1, -1, +1, -1\}$ in the presence of a Heisenberg perturbation. (a) Varying $\lambda$ for $V = 100$ or (b) varying $V$ for $\lambda = 0.1$ shows a controlled prethermal EE plateau $\propto \lambda^2/V^2$. The insets show the rescaled EE.

Sec. III A. The action of this perturbation is to toggle $+ \leftrightarrow -$ on a rung $i$. Under this operation, $\langle \hat{H}_V \rangle$ changes by $\approx 2Vc_i$, thus accessing a sector which is well separated in energy. This leads to a suppression due to Zeno dynamics, and a projection into the initial sector. We verify this numerically in Fig. 9(a), where we find a plateau at short to intermediate times for the EE which scales with $(\lambda/V)^2$. This is consistent with our results in Secs. III A and III B.

In comparison, under the application of the Heisenberg perturbation, the initial sector $+-+-+-$ can transition to, e.g., $++--+-$. This is in the same energy plateau, as our choice of $c_i \in \{+1, +1, +1, -1, -1, -1\}$ leads to a cancellation in the change in $\langle \hat{H}_V \rangle$ due to the double toggle. This can be seen by evaluating $\sum_i c_i \sigma_i^z \tau_i^z$ for both sectors and implies that the sector is unprotected. Furthermore, as the sector $++--+-$ has the same value of $\sigma_i^z \tau_i^z$ on either side of its center, the growth of EE is unrestricted, leading to vanilla saturation to an EE proportional to system size, with no dependence on $\lambda, V$. This is clearly seen in Fig. 9(b) for a range of values of $\lambda$. Here we have presented the protection of nontargeted sectors using a particular initial sector. However, the results hold for generic sectors as the protection is dependent on the matrix elements of the perturbation and not on the particular arrangement of the sector. Thus we are free to choose sectors based on the desired entanglement properties of the state to be protected.

### E. Thermodynamic limit (TDVP results)

For the ladder system studied here, the only perturbations that can lead to a buildup of entanglement across the middle of the chain are of the form $\pm\mp \leftrightarrow ++$ and $\pm\mp \leftrightarrow --$. Above, we show that the protection scheme controls the growth of entanglement entropy for small system sizes, with a clear scaling of the prethermal plateau and its lifetime. However, it is important to understand the effect of larger system sizes, as a larger Hilbert space may lead to a higher entropic pressure on the barrier to EE growth.

To confirm that our results for the 12-site system carry over to the thermodynamic limit, we study the dependence on system size. To this end, we employ the TDVP for matrix product states [43–46]. In general, it is intractable to study the long-time evolution of an interacting quantum many-body system, as it requires a prohibitively large bond dimension that usually grows exponentially in evolution time [47]. However, in our case, the protection term leads to constrained dynamics that requires a much smaller bond dimension, thus allowing us to access large system sizes. We perform the calculations for $N = 12, 20$, and $40$ for two different initial states perturbed by the transverse-field term and with an appropriate protection term. Figure 10 shows the result with one domain wall in the middle of the ladder and Fig. 11 shows the results with an alternating repeating domain wall, similar to the initial states discussed above. The maximum bond dimension is kept to $D = 200$ and maximum fidelity threshold $10^{-14}$ for $N = 40$. The calculations are performed using ITensor software library
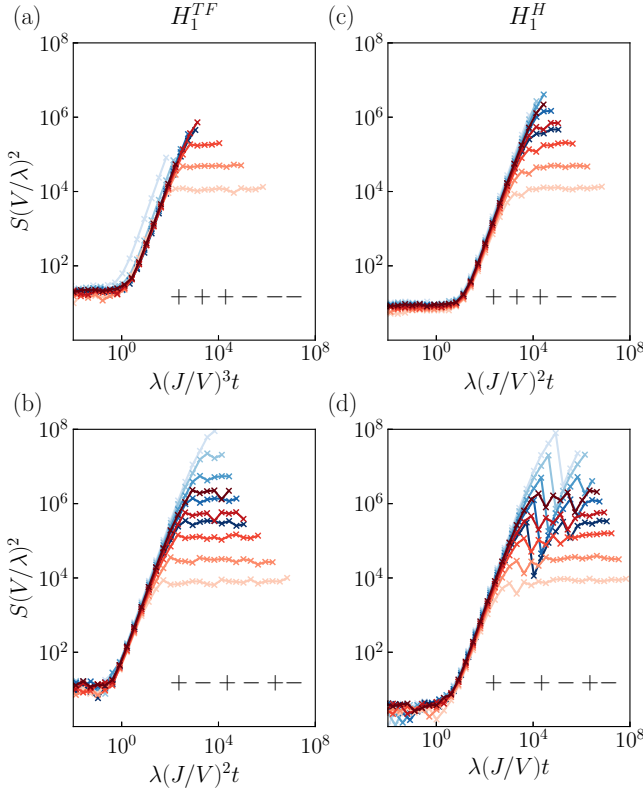
FIG. 8. Rescaled entanglement entropy growth with appropriate scaling in the presence of [(a) and (b)] transverse-field perturbation and [(c) and (d)] the Heisenberg perturbation when starting in [(a) and (c)] the $+++--$ sector or [(b) and (d)] the $+-+-+-$ sector. The blue and red curves are variations of $\lambda$ with fixed $V = 100$ and variations of $V$ with fixed $\lambda = 0.1$, respectively, with the same values used in Figs. 4–7.

[48]. The results confirm that the entanglement growth in the middle of chain remains almost unaffected with increasing system size.

## IV. SCALING RELATIONS FROM PERTURBATIVE ANALYSIS

The numerical results indicate the existence of two universal scaling relations. The first is the collapse with $(\lambda/V)^2$ of the EE plateau developed at intermediate to long times, and the second is the time at which the EE begins to increase again, which is seen to scale with the Hamiltonian parameters as $t \propto V/(J\lambda)$ in a worst-case scenario. Here we only attempt to understand the first scaling behavior, as it is tractable within first-order perturbation theory, while the second scaling behavior is understood from QZD [36]. The argument that we build in this section follows broadly the following structure: At first-order perturbation, there are no contributions from within the initial sector, and thus all contributing states have a suppression of $\mathcal{O}(\lambda/V)$. This translates to a contribution to the EE of $\mathcal{O}(\lambda^2/V^2)$ for the plateau. We argue this in detail below.

We carry out our analysis by considering the smallest possible system where we can study this behavior, namely a two-rung/four-site system. To understand the scaling of the
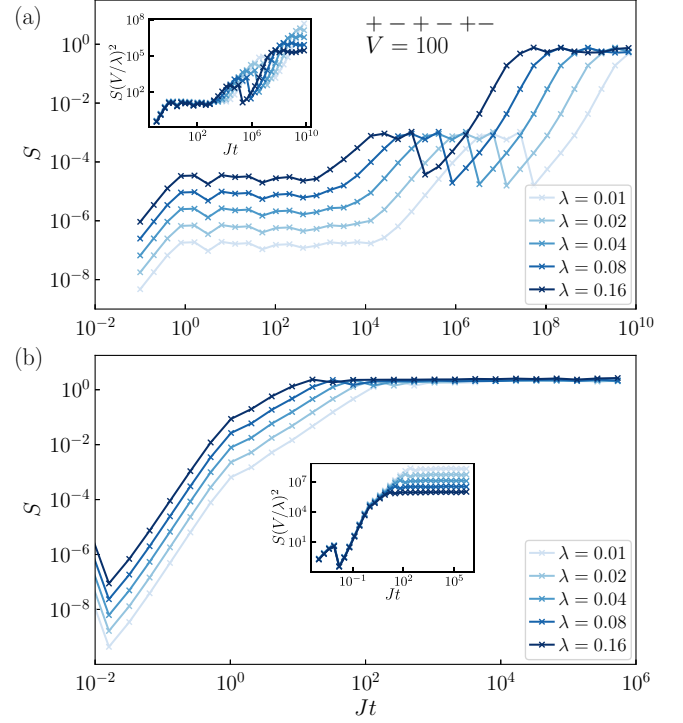


FIG. 9. Entanglement entropy growth for a product initial state in the sector $+-+-+-$ with $c_i \in \{+1, +1, +1, -1, -1, -1\}$ for (a) the transverse-field perturbation and (b) the Heisenberg perturbation with varying $\lambda$ for $V = 100$. The insets show the rescaled EE. This shows that even the "wrong" sequence $c_i$ can still adequately suppress EE growth for certain types of perturbations, but not generically.

EE plateau, let us consider an initial condition that belongs to the sector $+-$. The Hamiltonian in this sector can be rewritten in terms of broken segments, as defined in Sec. II, as $\hat{H}_0 = -\hat{\sigma}_1^x \hat{\tau}_1^x - \hat{\sigma}_2^x \hat{\tau}_2^x$. The eigenstates of this Hamiltonian are simply given by the product states of eigenstates of $\sigma_{1(2)}^x \tau_{1(2)}^x$. As the scaling we see in the previous section holds for generic product states, let us choose the ground state of this set to be our initial state, i.e., we begin with the state $\frac{1}{2}(|00\rangle + |11\rangle)_1(|01\rangle + |10\rangle)_2$ in $(\sigma, \tau)$ language. For convenience, from now on we will concatenate the basis states and express them as strings, for example the state discussed above will now be written as $\frac{1}{2}(|0001\rangle + |0010\rangle + |1101\rangle + |1110\rangle)$. Under the dynamics of just $\hat{H}_0 + \hat{H}_V$, this state is left unchanged as it is an eigenstate, and we shall call this as the initial state $|\psi_I\rangle$. We will also assume that $V \gg J, \lambda$, so that the sectors $+-, ++, --, -+$ have energies of $-2V, 0, 0, 2V$ respectively at leading order. Thus the sector under consideration is well separated from the others energetically.

Now let us consider the effect of a simple transverse-field perturbation $\hat{H}_1 = \lambda \sum_i (\hat{\sigma}_i^x + \hat{\tau}_i^x)$ on our Hamiltonian dynamics. At first order in $\lambda$, the eigenstates can be written as

$$|i'\rangle = |i\rangle + \lambda \sum_{j \neq i} \frac{1}{E_i - E_j} |j\rangle, \qquad (3)$$
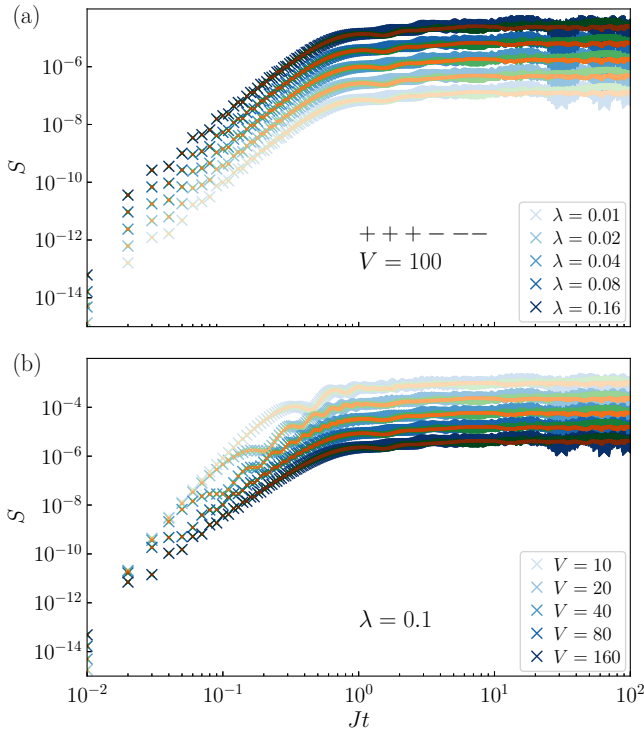
FIG. 10. Entanglement entropy growth for a product initial state in the sector $\ldots + + + - - - \ldots$ in the presence of the transverse-field perturbation with $c_i \in \{+1, +1, +1, -1, -1, -1\}$ for various system sizes calculated using TDVP. (a) Varying $\lambda$ for $V = 100$ or (b) varying $V$ for $\lambda = 0.1$, again shows suppression of the EE to a prethermal plateau $\propto \lambda^2/V^2$. Blue, green, and orange curves correspond to system sizes $N = 12, 20$, and $40$, respectively. The color shade gets darker with increasing values of $\lambda$ and $V$.
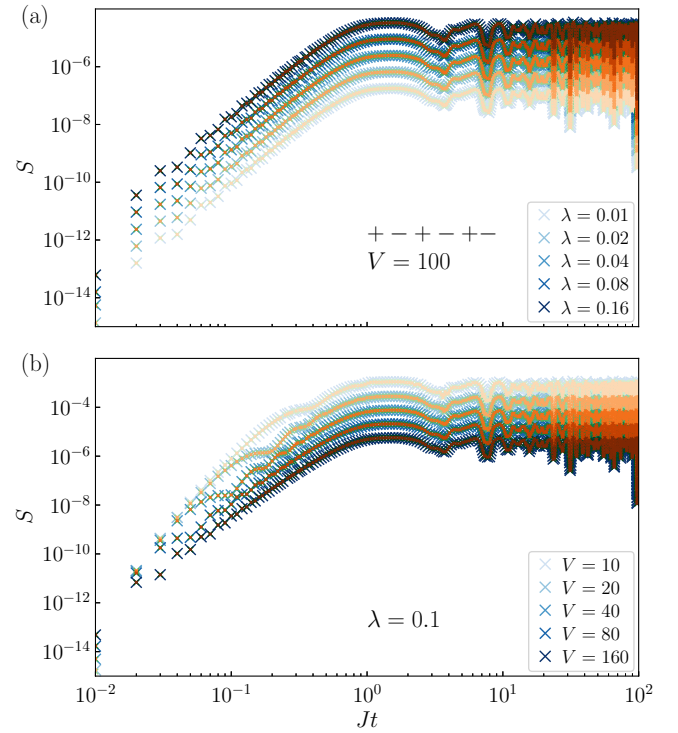


FIG. 11. Entanglement entropy growth for a product initial state in the sector $\ldots + - + - + - \ldots$ in the presence of the transverse-field perturbation with $c_i \in \{+1, -1, +1, -1, +1, -1\}$ for various system sizes. (a) Varying $\lambda$ for $V = 100$ or (b) varying $V$ for $\lambda = 0.1$ again shows a suppression of the EE into a prethermal plateau $\propto \lambda^2/V^2$. Blue, green, and orange curves correspond to system sizes $N = 12, 20$, and $40$, respectively. The color shade gets darker with increasing values of $\lambda$ and $V$.

where the perturbed (original) basis is denoted by $|i'\rangle(|i\rangle)$. Note that the energy separation in the sector structure as discussed above renders all $|j\rangle \neq |i\rangle$ contributing to the above expression to have a coefficient of $\lambda/V$, as the perturbation is *sector off-diagonal*, i.e., it has no nonzero matrix elements within the sectors as defined by $\hat{H}_0$. For ease of notation, let us express Eq. (3) as $|i'\rangle = \sum_i M_{i'i}|i\rangle$. The relation between the perturbed and original basis can also be similarly written using first-order perturbation theory as $|i\rangle = \sum_{i'} M'_{ii'}|i'\rangle$, and we will make use of both these expression to understand the EE.

To understand the time evolution of our initial product state, let us first express $e^{-i\hat{H}t}|0\rangle$, where $\hat{H} = \hat{H}_0 + \hat{H}_1 + \hat{H}_V$ and $|0\rangle$ now denotes the initial state in the original basis, as $\sum_{i'} e^{-iE'_{i'}t} M'_{0i'}|i'\rangle$. As the EE is measured in the original basis by partitioning the lattice, we replace the dependence on the perturbed basis and rewrite the time evolved state as $\sum_{i',j} e^{-iE'_{i'}t} M'_{0i'} M_{i'j}|j\rangle$. At intermediate times, we can consider the phase factor to be sufficiently uncorrelated, and the dependence on $\lambda/V$ can be read directly from the $M'_{0i'} M_{i'j}$ terms, as no constructive or destructive interference is to be expected. Of these, the largest coefficient would be $M'_{00'} M_{0'0}$, which is $\mathcal{O}(1)$. To understand the other coefficients, let us reiterate a key property of both $M$ and $M'$, namely that if the matrix element corresponding to $i, i'$ ($i', j$) is nonzero, then it

is $\mathcal{O}(1)$ if $i = i'$ ($i' = j$), and $\lambda/V$ (to leading order) if not. This implies that for terms of order $\lambda/V$, we only need to consider coefficients from matrix elements $M'_{00} M_{0j}$ and $M'_{0i'} M_{i'i'}$. As $M$ ($M'$) can only connect states within the starting sector to those outside, we can write our resulting state after time evolution for an intermediate time as $|\psi_I\rangle + (\lambda/V) \sum_\alpha c_\alpha |\alpha\rangle$, where $\alpha$ lists states outside the sector of interest.

The calculation of the half-chain EE of such a state will first require a reduced density matrix. For the remainder of this section, we shall use $c = \lambda/V$ for ease of notation. The reduced density matrix for the state discussed above can be expressed (to leading order) as

$$
\hat{\rho}_A = \begin{pmatrix} 0.5 & ac & ac & 0.5 \\ ac & bc^2 & 0 & ac \\ ac & 0 & bc^2 & ac \\ 0.5 & ac & ac & 0.5 \end{pmatrix}, \tag{4}
$$

where $a$ and $b$ are prefactors coming from the perturbative expansion, and the rows correspond to the left rung configurations 00, 01, 10, and 11, respectively. Diagonalizing this matrix reduces the von Neumann entropy $-\text{Tr}[\hat{\rho}_A \log(\hat{\rho}_A)]$ to $-\sum_i E_i \log(E_i)$. The eigenvalues to $\mathcal{O}(c^2)$ are $0, bc^2, a'c^2, 1 + b'c^2$, where $a'$ and $b'$ are functions of $a$ and $b$. For the second and third eigenvalues, $E_i \log(E_i)$ reduces
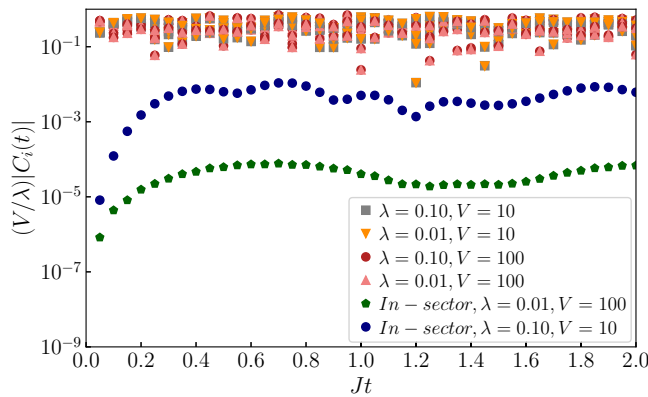
FIG. 12. Wave-function coefficients for relevant states as a function of time for a four-rung system. For the four nonequivalent states out of sector, we see that a scaling with $\lambda/V$ leads to data collapse over a single decade, whereas for in-sector states (only those with the largest coefficients shown), we clearly see that the scaling is not sufficient and that we require a higher power of $\lambda/V$ as expected. Note that the largest in-sector wave-function coefficients are doubly degenerate.

to the form $bc^2[2\log(c) + \log(b)]$, and the scaling with $c$ is controlled approximately only by $c^2$, as the logarithm function is insensitive to variations in $c$ for $c \ll 1$. For the last eigenvalue, we can expand around unity, as $c \ll 1$, and this leads to $E_i \log(E_i) \approx \mathcal{O}(c^2)$. Thus we see that the overall scaling of the von Neumann EE is controlled by $c^2$, i.e., $(\lambda/V)^2$.

As the above analysis is for a two-rung system, and carrying out the same argument for a larger system size quickly becomes analytically intractable, we would like to confirm that the assumption about the state at time $t$, which we have made above, holds true. This would justify our expectation that a similar argument extends to the thermodynamic limit. For ease of understanding, let us assume that we initialize our state as the ground state in the sector $+-+-$. This is again a product state of the symmetric eigenvector of $\sum_i \hat{\sigma}_i^x \hat{\tau}_i^x$. Explicitly, our initial state is now

$$|\psi_I\rangle = \tfrac{1}{4}(|00\rangle + |11\rangle)_1(|01\rangle + |10\rangle)_2(|00\rangle + |11\rangle)_3(|01\rangle + |10\rangle)_4,$$
(5)

where the subscript denotes the rung number. On expanding the above expression, it is easy to see that this is a uniform superposition over the 16 basis states making up the sector $+-+-$. To ensure that other states within this sector do not participate in the time evolution, we can plot the coefficients of the 16 basis states, and if they stay equal throughout the time evolution for the period of interest, we can conclude that the other in-sector states can be neglected. For the states that are connected at first order in perturbation theory, careful observation of the structure of the Hamiltonian in state space shows a number of states that have equivalent dynamic behavior. We choose four nonequivalent states out of these: $|01010001\rangle$, $|10010001\rangle$, $|00000001\rangle$, and $|00110001\rangle$. We expect to find that the coefficients of these states are $\propto (\lambda/V)$. The results for the coefficients discussed above from our exact numerics are shown in Fig. 12, and indeed we find that (i) the coefficients of the 15 in-sector eigenstates of

$H_0$ require a higher power of $V/\lambda$ to get a scaling collapse, implying that in-sector states play no role at first order, and (ii) the four out-of-sector states discussed above have a coefficient that scales with $(\lambda/V)$. Thus we find that the assumptions of our perturbative analysis are correct and that we can expect the results to extend to larger system sizes.

## V. CONCLUSIONS

We have investigated a fine-tuned many-body spin system, which behaves as a system of smaller noninteracting subsystems due to a classical degeneracy in intersite interactions and carefully engineered local conserved quantities. While the former is expected to occur for generic insulating crystals due to space group symmetries, the latter severely restricts the form of quantum fluctuations available to the system. Thus we have studied the effect of generic perturbations (of strength $\lambda$) that destroy the local conservation and lead to a standard growth in entanglement with increasing evolution time, as would be expected for a generic quantum many-body system.

To recover features of our disentangled dynamics, we impose a large energy separation $V$ via a sector protection term between the sector (indexed by the values of the local conserved quantities) of interest and the rest of the spectrum. This effectively isolates our sector dynamically, leading to a suppression of the effect of the perturbation which couples various sectors. Numerical investigations show that the entanglement developed is effectively controlled by $\lambda/V$, where the entanglement entropy settles into a prethermal plateau $\propto \lambda^2/V^2$ up to timescales polynomial in $V$. We justify this behavior via a first-order perturbative analysis. Although our protective term is chosen to be specific to the sector we want to protect, we also see that there is an accidental protection of other sectors that have the disentangled structure. This is specific to the form of the perturbation, which is unable to mix sectors within the same energy plateau at first order and as higher-order contributions are suppressed by the energy scale $V$. However, we also see that for different forms of the perturbation, which are able to transition between sectors in the same energy plateau, the entanglement reaches its saturation value in time $\propto$ system size.

Our approach differs from other studies of prethermal behavior, as the generic feature identified in such cases is usually the deviation from a random state at the same energy density for a parametrically long time. In addition to this general feature, the state which our model generates in the prethermal regime is highly structured and is qualitatively much closer to a product state, than to a featureless generic prethermal state. This difference highlights the novel effects of the unperturbed Hamiltonian which we are able to preserve even in the presence of generic perturbations. The example that we have studied demonstrates the significance of this special fine-tuned point in parameter space and the extent to which it can control the dynamics in a perturbative regime. This can easily be extended to larger systems and geometries in higher dimensions, as the local conserved quantity acts only on-site. Given that spin systems are realized in generic insulating crystals, it is also possible to find anisotropic crystals of the XXZ type which would be proximate to the Hamiltonian discussed here.

Finally, let us point out that this mechanism can prove to be extremely useful for quantum computing setups where one wishes to eliminate unwanted interactions between qubits. Thus, future directions include designing gates for this rung architecture and considering possible experimental platforms where we may be able to realize such physics.

## ACKNOWLEDGMENTS

[1] L. D'Alessio, Y. Kafri, A. Polkovnikov, and M. Rigol, From quantum chaos and eigenstate thermalization to statistical mechanics and thermodynamics, Adv. Phys. **65**, 239 (2016).

[2] J. M. Deutsch, Eigenstate thermalization hypothesis, Rep. Prog. Phys. **81**, 082001 (2018).

[3] J. M. Deutsch, Quantum statistical mechanics in a closed system, Phys. Rev. A **43**, 2046 (1991).

[4] M. Srednicki, Chaos and quantum thermalization, Phys. Rev. E **50**, 888 (1994).

[5] M. Rigol, V. Dunjko, and M. Olshanii, Thermalization and its mechanism for generic isolated quantum systems, Nature (London) **452**, 854 (2008).

[6] D. M. Basko, I. L. Aleiner, and B. L. Altshuler, Metal–insulator transition in a weakly interacting many-electron system with localized single-particle states, Ann. Phys. **321**, 1126 (2006).

[7] I. V. Gornyi, A. D. Mirlin, and D. G. Polyakov, Interacting electrons in disordered wires: Anderson localization and low-$t$ transport, Phys. Rev. Lett. **95**, 206603 (2005).

[8] R. Nandkishore and D. A. Huse, Many-body localization and thermalization in quantum statistical mechanics, Annu. Rev. Condens. Matter Phys. **6**, 15 (2015).

[9] D. A. Abanin, E. Altman, I. Bloch, and M. Serbyn, Colloquium: Many-body localization, thermalization, and entanglement, Rev. Mod. Phys. **91**, 021001 (2019).

[10] F. Alet and N. Laflorencie, Many-body localization: An introduction and selected topics, C. R. Phys. **19**, 498 (2018).

[11] E. van Nieuwenburg, Y. Baum, and G. Refael, From bloch oscillations to many-body localization in clean interacting systems, Proc. Natl. Acad. Sci. USA **116**, 9269 (2019).

[12] M. Schulz, C. A. Hooley, R. Moessner, and F. Pollmann, Stark many-body localization, Phys. Rev. Lett. **122**, 040606 (2019).

[13] A. Smith, J. Knolle, D. L. Kovrizhin, and R. Moessner, Disorder-free localization, Phys. Rev. Lett. **118**, 266601 (2017).

[14] M. Brenes, M. Dalmonte, M. Heyl, and A. Scardicchio, Many-body localization dynamics from gauge invariance, Phys. Rev. Lett. **120**, 030601 (2018).

[15] J. C. Halimeh, P. Hauke, J. Knolle, and F. Grusdt, Temperature-induced disorder-free localization, arXiv:2206.11273.

[16] N. Chakraborty, M. Heyl, P. Karpov, and R. Moessner, Disorder-free localization transition in a two-dimensional lattice gauge theory, Phys. Rev. B **106**, L060308 (2022).

[17] N. Chakraborty, M. Heyl, P. Karpov, and R. Moessner, Spectralresponse of disorder-free localized lattice gauge theories, arXiv:2211.14328.

[18] H. Bernien, S. Schwartz, A. Keesling, H. Levine, A. Omran, H. Pichler, S. Choi, A. S. Zibrov, M. Endres, M. Greiner, V. Vuletić, and M. D. Lukin, Probing many-body dynamics on a 51-atom quantum simulator, Nature (London) **551**, 579 (2017).

[19] F. M. Surace, P. P. Mazza, G. Giudici, A. Lerose, A. Gambassi, and M. Dalmonte, Lattice gauge theories and string dynamics in Rydberg atom quantum simulators, Phys. Rev. X **10**, 021041 (2020).

[20] C. J. Turner, A. A. Michailidis, D. A. Abanin, M. Serbyn, and Z. Papić, Weak ergodicity breaking from quantum many-body scars, Nat. Phys. **14**, 745 (2018).

[21] S. Moudgalya, S. Rachel, B. A. Bernevig, and N. Regnault, Exact excited states of nonintegrable models, Phys. Rev. B **98**, 235155 (2018).

[22] P. Sala, T. Rakovszky, R. Verresen, M. Knap, and F. Pollmann, Ergodicity breaking arising from hilbert space fragmentation in dipole-conserving Hamiltonians, Phys. Rev. X **10**, 011047 (2020).

[23] V. Khemani, M. Hermele, and R. Nandkishore, Localization from hilbert space shattering: From theory to physical realizations, Phys. Rev. B **101**, 174204 (2020).

[24] T. Rakovszky, P. Sala, R. Verresen, M. Knap, and F. Pollmann, Statistical localization: From strong fragmentation to strong edge modes, Phys. Rev. B **101**, 125126 (2020).

[25] S. Moudgalya and O. I. Motrunich, Hilbert space fragmentation and commutant algebras, Phys. Rev. X **12**, 011050 (2022).

[26] G. De Tomasi, D. Hetterich, P. Sala, and F. Pollmann, Dynamics of strongly interacting systems: From fock-space fragmentation to many-body localization, Phys. Rev. B **100**, 214313 (2019).

[27] Z.-C. Yang, F. Liu, A. V. Gorshkov, and T. Iadecola, Hilbert-space fragmentation from strict confinement, Phys. Rev. Lett. **124**, 207602 (2020).

[28] J.-Y. Desaules, G.-X. Su, I. P. McCulloch, B. Yang, Z. Papić, and J. C. Halimeh, Ergodicity breaking under confinement in cold-atom quantum simulators, arXiv:2301.07717.

[29] S. Scherg, T. Kohlert, P. Sala, F. Pollmann, B. H. Madhusudhana, I. Bloch, and M. Aidelsburger, Observing non-ergodicity due to kinetic constraints in tilted fermi-hubbard chains, Nat. Commun. **12**, 4490 (2021).

[30] T. Kohlert, S. Scherg, P. Sala, F. Pollmann, B. H. Madhusudhana, I. Bloch, and M. Aidelsburger, Exploring the regime of fragmentation in strongly tilted fermi-hubbard chains, Phys. Rev. Lett. **130**, 010201 (2023).

[31] P. Patil and A. W. Sandvik, Hilbert space fragmentation and ashkin-teller criticality in fluctuation coupled ising models, Phys. Rev. B **101**, 014453 (2020).

[32] S. Moudgalya, B. A. Bernevig, and N. Regnault, Quantum many-body scars and hilbert space fragmentation: a review of exact results, Rep. Prog. Phys. **85**, 086501 (2022).

[33] P. Facchi and S. Pascazio, Quantum zeno subspaces, Phys. Rev. Lett. **89**, 080401 (2002).

[34] P. Facchi, D. A. Lidar, and S. Pascazio, Unification of dynamical decoupling and the quantum zeno effect, Phys. Rev. A **69**, 032314 (2004).

[35] P. Facchi, G. Marmo, and S. Pascazio, Quantum zeno dynamics and quantum zeno subspaces, J. Phys.: Conf. Ser. **196**, 012017 (2009).

[36] D. Burgarth, P. Facchi, H. Nakazato, S. Pascazio, and K. Yuasa, Generalized adiabatic theorem and strong-coupling limits, Quantum **3**, 152 (2019).

[37] W. Brzezicki, J. Dziarmaga, and A. M. Oleś, Quantum phase transition in the one-dimensional compass model, Phys. Rev. B **75**, 134415 (2007).

[38] W. Brzezicki and A. M. Oleś, Exact solution for a quantum compass ladder, Phys. Rev. B **80**, 014405 (2009).

[39] O. Hart, S. Gopalakrishnan, and C. Castelnovo, Logarithmic entanglement growth from disorder-free localization in the two-leg compass ladder, Phys. Rev. Lett. **126**, 227202 (2021).

[40] J. C. Halimeh, L. Homeier, H. Zhao, A. Bohrdt, F. Grusdt, P. Hauke, and J. Knolle, Enhancing disorder-free localization through dynamically emergent local symmetries, PRX Quantum **3**, 020345 (2022).

[41] H. Kim and D. A. Huse, Ballistic spreading of entanglement in a diffusive nonintegrable system, Phys. Rev. Lett. **111**, 127205 (2013).

[42] D. N. Page, Average entropy of a subsystem, Phys. Rev. Lett. **71**, 1291 (1993).

[43] J. Haegeman, C. Lubich, I. Oseledets, B. Vandereycken, and F. Verstraete, Unifying time evolution and optimization with matrix product states, Phys. Rev. B **94**, 165116 (2016).

[44] J. Haegeman, J. I. Cirac, T. J. Osborne, I. Pižorn, H. Verschelde, and F. Verstraete, Time-dependent variational principle for quantum lattices, Phys. Rev. Lett. **107**, 070601 (2011).

[45] L. Vanderstraeten, J. Haegeman, and F. Verstraete, Tangent-spacemethods for uniform matrix product states, SciPost Phys. Lect. Notes 7 (2019).

[46] E. Leviatan, F. Pollmann, J. H. Bardarson, D. A. Huse, and E. Altman, Quantum thermalization dynamics with matrix-product states, arXiv:1702.08894.

[47] U. Schollwöck, The density-matrix renormalization group in the age of matrix product states, Ann. Phys. **326**, 96 (2011).

[48] M. Fishman, S. R. White, and E. M. Stoudenmire, The ITensor software libraryfor tensor network calculations, SciPost Phys. Codebases 4 (2022).